J. Fluid Mech. (2008), *vol.* 612, *pp.* 387–406.
doi:10.1017/S0022112008003042 Printed in the United Kingdom

Spectral properties and universal behaviour of advecting–diffusing scalar fields in finite-length channels

M. GIONA[1], S. CERBELLI[1] AND F. CRETA[2]

[1]Dipartimento di Ingegneria Chimica, Università di Roma "La Sapienza", via Eudossiana 18, 00184 Roma

[2]Dipartimento di Meccanica ed Aeronautica, Università di Roma "La Sapienza", via Eudossiana 18, 00184 Roma

(Received 7 May 2007 and in revised form 19 June 2008)

This paper analyses the relaxation towards the steady state of an advecting–diffusing field in a finite-length channel. The dominant eigenvalue, $-\Lambda_F$, of the advection–diffusion operator provides the slowest relaxation time scale for achieving steady state in open flow devices. We focus on parallel flows and analyse how Λ_F depends on the velocity profile and the molecular diffusivity. As a result of the universal localization features of the eigenfunction associated with Λ_F, we find that Λ_F can be predicted analytically based on the local behaviour of the velocity profile near the stagnation points. Microfluidic applications of the theory are also addressed.

1. Introduction

The appropriate mathematical formulation for the physics of single-phase scalar mixing in an incompressible flow is described by the scalar field equation,

$$\frac{\partial \phi}{\partial t} = -\nabla \cdot (\boldsymbol{v}\phi) + D\nabla^2\phi = \mathscr{L}_{\boldsymbol{v},D}[\phi], \tag{1.1}$$

where ϕ is the scalar concentation, D is the diffusivity of the transported entity, and the velocity field $\boldsymbol{v}$ is solenoidal ($\nabla \cdot \boldsymbol{v} = 0$). The properties of the solutions of (1.1) are strongly related to the nature of the domain where the mixing process occurs.

Three broad categories can be identified, namely unbounded domains (e.g. $\mathbb{R}^2$ or the ordinary space $\mathbb{R}^3$), closed bounded domains (e.g. a closed stirred vessel), and open bounded domains (e.g. inflow–outflow systems such as static mixers or microchannels). The better understood case is that of unbounded domains. In this context, a consistent theory (homogenization theory) has been derived for a variety of two-dimensional convective flows possessing a periodic (Fannjiang & Papanicolaou 1994) or random (Fannjiang & Papanicolaou 1997) cellular structure. This theory predicts that the spatiotemporal asymptotic behaviour of (1.1) approaches that of a pure diffusion equation with constant tensor diffusivity. A physical consequence of this property is that the time asymptotic contour levels of an initial scalar field with compact support (e.g. a Dirac's pulse) approach that of an ellipses whose principal axes grow proportional to $\sqrt{t}$. The proportionality constants depend upon the interaction between the specific structure of the velocity field and diffusional motion. Alternative approaches to mixing in two-dimensional unbounded domains in

the presence of time-periodic flows make explicit use of Lagrangian templates such as invariant manifolds in place of the Eulerian description of the velocity streamfunction (Beigie Leonard & Wiggins 1991). For further details see e.g. the review paper by Majda & Kramer (1999).

While in unbounded domains the dynamics of a scalar field ϕ is indicative of the dispersion properties, in bounded domains the mixing action deriving from the interplay between advection and diffusion is aimed at homogenizing ϕ within the mixing space Ω. The techniques used for investigating dispersion in unbouded domains, be they Eulerian or Lagrangian, are of little use in the case where the mixing space Ω is bounded, in that the boundary conditions prescribed on the boundary $\partial\Omega$ have a direct impact on the time asymptotic properties of $\phi(\boldsymbol{x}, t)$.

If the domain is bounded and closed, and therefore the walls are impermeable to the advecting–diffusing scalar (i.e. $\boldsymbol{J}\cdot\boldsymbol{n}=0$ on $\partial\Omega$, where $\boldsymbol{J}=\boldsymbol{v}\phi - D\nabla\phi$, and $\boldsymbol{n}$ is a unit outward-pointing vector normal to $\partial\Omega$), then, as $t\to\infty$, the scalar field approaches a spatially uniform structure $\phi(\boldsymbol{x}, t)\to\phi_0=(\int_\Omega \phi(\boldsymbol{x}, 0)\,\mathrm{d}\boldsymbol{x})/\mathrm{meas}(\Omega)$, where $\mathrm{meas}(\Omega)$ is the (Lebesgue) measure of the mixing space.

In this situation, quantifying mixing efficiency (i.e. homogenization dynamics) consists of determining the spectral structure associated with the advection–diffusion operator $\mathscr{L}_{\boldsymbol{v},D}$ if the flow is autonomous, or with the associated Floquet operator, in the case where the velocity field is time-periodic (Giona *et al.* 2004*a*).

Several articles have focused on the structure of the spatial patterns in periodically advecting–diffusing systems (Pierrehumbert 1994), showing that, in the presence of small diffusivity, the eigenfunctions of the Floquet operator, or of the Frobenius–Perron operator associated with advection with small noise superimposed, are localized in the non-mixing region of the flow (Pikovsky & Popovych 2003; Giona *et al.* 2004*a*). The effect of different boundary conditions on the structure of the eigenfunctions of the advection–diffusion operator has been addressed in Gilbert (2006) and in Chertkov & Lebedev (2003) in regard to advecting–diffusing and reacting systems. Most of these contributions have approached the analysis of advecting–diffusing systems by considering the pulsed-system approximation, which is obtained by splitting the simultaneous action of advection and diffusion into two separate steps: a first step in which advection is active and no diffusion occurs, and a second step without advection, in which solely the action of diffusion acts on the scalar field (Pierrehumbert 1994; Pikovsky & Popovych 2003; Gilbert 2006). The limits of applicability of this technique have been addressed in Backus (1958) and more recently in Giona, Androver & Cerbelli (2005).

Focusing on the autonomous case, the positive character of $\mathscr{L}_{\boldsymbol{v},D}$, expressed by the fact that if $\phi(\boldsymbol{x}, 0)\geqslant 0$ then $\phi(\boldsymbol{x}, t)\geqslant 0$ at all times $t>0$, implies the existence of a real eigenvalue $-\Lambda_F$, referred to as the Frobenius eigenvalue, which corresponds to mass conservation, and of its associated real-valued eigenfunction, $\psi_F(\boldsymbol{x})$. In the case of bounded closed domains, $\Lambda_F=0$, and $\psi_F(\boldsymbol{x})=1_\Omega$, where 1_Ω is a constant unit function defined in Ω. In other words, the Frobenius eigenvalue is associated with the trivial uniformly mixed state. The main quantity assessing the mixing efficiency is therefore the second dominant eigenvalue, say $-\Lambda_1=-\lambda_1+\mathrm{i}\,\omega_1$, associated with $\mathscr{L}_{\boldsymbol{v},D}$, defined as the eigenvalue whose real part possesses the lowest – strictly positive – absolute value. The reciprocal of λ_1 provides the slowest relaxation time scale towards the uniformly mixed state. Note that the extension of these observations to time-periodic closed flows requires only obvious modifications when applied to the Floquet operator in place of $\mathscr{L}_{\boldsymbol{v},D}$. Specifically, $-\Lambda_F=1$, and the dominant eigenvalue is defined as the eigenvalue, different from Λ_F, possessing the highest modulus.

A point of primary interest is then to establish how λ_1 depends on the velocity field $\boldsymbol{v}$ and on the diffusivity D, especially in the limit of vanishing noise, $D \to 0$. It can be observed that the intermediate-time-scale dynamics may show significant deviations from the asymptotic exponential scaling as discussed in Popovych, Pikovsky & Eckhardt (2007).

In a previous paper (Giona, Cerbelli & Vitacolonna 2004*b*), a closed-form expression of such dependence was obtained for the case of steady parallel flows. It was found that $\lambda_1 \sim D^{\alpha}$, where the exponent α depends on the local structure of the velocity field near its extremal point (relative maxima and minima). Specifically, the results is $\alpha = 1/2$ whenever the velocity profile is locally quadratic, a situation that occurs in the vast majority of cases.

The theoretical analysis of open-flow systems is not as well developed as for closed flows, though several interesting results have been obtained (Tel *et al.* 2005; Straube & Pikovsky 2007).

In this article, we analyse the case of open bounded flows, where the scalar ϕ is continuously fed to an inlet section and withdrawn at an outlet section of a finite length two-dimensional channel. Specifically, we focus on the relaxation properties towards the steady-state condition in the inflow/outflow system. The theory presented can be considered as the extension of the results reported in Giona *et al.* (2004*b*) to open bounded flow devices.

Different velocity profiles including plug flow, Poiseuille, and shear flows are considered. The main difference with respect to closed domains is that the quantity $\int_{\Omega} \phi(\boldsymbol{x}, t)\, \mathrm{d}\boldsymbol{x}$ is not conserved for open systems, and consequently the focus is oriented towards predicting the Frobenius eigenvalue $\Lambda_F \neq 0$ itself, which, for this type of system, provides the slowest relaxation time scale towards steady state associated with a generic initial loading and with a prescribed feeding condition.

The article is organized as follows. Section 2 defines the problem formally and introduces the concept of the Frobenius eigenvalue. Section 3 compares and contrasts the present analysis with the phenomenon of Taylor–Aris dispersion in tubes. Section 4 develops the spectral theory for bounded open flows, defines the universality properties and compares the theory with detailed numerical simulations. Section 5 describes further results supporting the theory and addresses some of its practical fluid dynamic implications.

2. Statement of the problem

Let the rectangular channel be represented by $0 \leqslant x \leqslant L$, $0 \leqslant y \leqslant W$ ($y = 0$ and $y = W$ represent the channel walls), and let the velocity field be given by $\boldsymbol{v} = (u(y), 0)$, $u(y) \geqslant 0$. By introducing the dimensionless variables $(x, y) \to (x/L, y/W)$, $t \to tL/V_c$, $\boldsymbol{v} \to \boldsymbol{v}/V_c$, where V_c is a reference velocity such that the resulting dimensionless flow possesses unit flow rate, the advection–diffusion equation (1.1) becomes

$$\frac{\partial \phi}{\partial t} = -u(y)\frac{\partial \phi}{\partial x} + \varepsilon\left(\frac{\partial^2 \phi}{\partial x^2} + \alpha^2 \frac{\partial^2 \phi}{\partial y^2}\right) = \mathscr{L}_{\boldsymbol{v},\varepsilon,\alpha}[\phi] \tag{2.1}$$

where $\alpha = L/W \geqslant 1$ is the aspect ratio of the channel, and $\varepsilon = 1/Pe$, where $Pe = V_c L/D$ is the Péclet number. In order to simplify the notation, we use the same symbols $\boldsymbol{x} = (x, y)$, $\boldsymbol{v} = (u, v)$ to indicate the corresponding dimensionless quantities, with the understanding that only the dimensionless formulation of the problem will be considered henceforth.

Equation (2.1) is given with the initial condition $\phi(\boldsymbol{x},0)=\phi_0(\boldsymbol{x})$, with boundary conditions

$$\left.\frac{\partial\phi}{\partial y}\right|_{y=0} = \left.\frac{\partial\phi}{\partial y}\right|_{y=1} = 0 \tag{2.2}$$

at the channel walls, and the conditions

$$\phi|_{x=0} = \phi_i(y), \qquad \left.\frac{\partial\phi}{\partial x}\right|_{x=1} = 0 \tag{2.3}$$

at the inlet and outlet sections, respectively. Specifically, the outlet condition expresses the classical Danckwerts conditions at the outlet section (Danckwerts 1953). Other types of inlet/outlet boundary conditions have been proposed (Smith 1988), which are not of general applicability, and can be used essentially only for one-dimensional models.

The right hand-side of (2.1) defines the advection–diffusion operator $\mathscr{L}_{\boldsymbol{v},\varepsilon,\alpha}$, which is a positive operator (Farina & Rinaldi 2000), i.e. if the inlet and initial conditions are non-negative, then the solution is non-negative for any $t>0$. The operator $\mathscr{L}_{\boldsymbol{v},\varepsilon,\alpha}$ possesses a countable set of eigenvalues all with strictly negative real part.

The positive character of $\mathscr{L}_{\boldsymbol{v},\varepsilon,\alpha}$ implies that its dominant eigenvalue (i.e. the eigenvalue whose real part possesses lowest absolute value) is real and of multiplicity equal to 1. Its associated eigenfunction can always be chosen to be non-negative. This eigenvalue, which we denote as $-\Lambda_F$ ($\Lambda_F>0$), provides the slowest time scale describing the exponential relaxation towards the steady-state profile $\phi_{ss}(\boldsymbol{x})$,

$$\phi(\boldsymbol{x},t)-\phi_{ss}(\boldsymbol{x}) \simeq \psi_F(\boldsymbol{x})\mathrm{e}^{-\Lambda_F t}, \qquad t\to\infty, \tag{2.4}$$

associated with generic initial and inlet conditions. The function $\psi_F(\boldsymbol{x})$ entering (2.4), is the Frobenius eigenfunction associated with $-\Lambda_F$.

Therefore, the study of the relaxation towards the steady state of a scalar field in bounded open flow systems consists of analysing the dependence of Λ_F on Pe and on the flow field $u(y)$.

While in closed flow systems the real part of the eigenvalue $-\Lambda_1$ is a measure of the mixing efficiency, the eigenvalue $-\Lambda_F$ is a measure of the time scales required to reach steady conditions. Thus, while $-\Lambda_F$ is not in itself a measure of mixing efficiency, which in steady state can be obtained by studying the properties of $\phi_{ss}(\boldsymbol{x})$ entering (2.4), it provides preliminary information that is essential for motivating the analysis of steady-state mixing. For instance, a time scale excessively long, i.e. a small value of $-\Lambda_F$, suggests that a steady-state assessment of mixing efficiency might be unphysical and that the whole transient behaviour should be considered.

3. Relaxation dynamics and Taylor–Aris dispersion

In the case of a flat velocity profile, i.e. $u(y)=1$, the advection–diffusion operator becomes

$$\mathscr{L}_{\boldsymbol{v},\varepsilon,\alpha}[\phi] = -\frac{\partial\phi}{\partial x} + \frac{1}{Pe}\nabla_\alpha^2\phi, \tag{3.1}$$

where $\nabla_\alpha^2=(\partial^2/\partial x^2+\alpha^2\partial^2/\partial y^2)$. In order to obtain a proper setting for the eigenvalue problem associated with (2.1), let us homogenize the boundary condition by setting $\psi(\boldsymbol{x})=\phi(\boldsymbol{x})-\phi_{ss}(\boldsymbol{x})$, where $\phi_{ss}(\boldsymbol{x})$ is the steady-state solution, so that $\psi(\boldsymbol{x})$ satisfies

(3.1) with the homogeneous conditions

$$\left.\frac{\partial\psi}{\partial y}\right|_{y=0} = \left.\frac{\partial\psi}{\partial y}\right|_{y=1} = 0, \qquad \psi|_{x=0} = 0, \qquad \left.\frac{\partial\psi}{\partial x}\right|_{x=1} = 0. \tag{3.2}$$

By setting $\psi(x, y) = q(x)\cos(n\pi y)$ in the eigenvalue/eigenfunction problem $\mathscr{L}_{\boldsymbol{v},\varepsilon,\alpha}[\psi] = \lambda\psi$, one obtains for the auxiliary function $q(x)$ the equation

$$q''(x) - Pe\, q'(x) - Pe\beta q(x) = 0, \tag{3.3}$$

where $q'(x) = \mathrm{d}q(x)/\mathrm{d}x$, $\beta = \alpha^2 n^2\pi^2/Pe + \lambda$, and the function $q(x)$ should satisfy the boundary conditions $q(x)|_{x=0} = 0$, $q'(x)|_{x=1} = 0$.

The second-order equation in $q(x)$, (3.3), together with its boundary conditions provides a countable set of one-dimensional eigenvalue-eigenfunction problems, which admit the solution $q_m(x) = \mathrm{e}^{Pex/2}\sin(\omega_m x)$, $m = 1, 2, \ldots$, where the ω_m form an increasing sequence of positive numbers fulfilling the cardinal equation $\tan(\omega_m) = -2\omega_m/Pe$. Specifically, at large Pe, $\omega_m \simeq (2m - 1)\pi/2$. The eigenvalue spectrum $\{\lambda_{n,m}\}$ of the advection–diffusion operator is therefore given by

$$-\lambda_{n,m} = \frac{\omega_m^2 + \alpha^2 n^2\pi^2}{Pe} + \frac{Pe}{4}, \qquad n = 0, 1, \ldots, m = 1, 2, \ldots. \tag{3.4}$$

Therefore, the Frobenius eigenvalue is obtained for $n = 0$ and $m = 1$ and is

$$\Lambda_F = \frac{\omega_1^2}{Pe} + \frac{Pe}{4} \tag{3.5}$$

and the associated eigenfunction is expressed by $\psi_F(x, y) = \mathrm{e}^{Pex/2}\sin(\omega_1 x)$. The dominant Frobenius eigenfunction is excited by any inlet condition possessing a non-vanishing mean. Inlet conditions possessing zero mean excite the next dominant eigenvalue of the spectrum, which is given by $\Lambda_1 = -\lambda_{1,1} = (\omega_1^2 + \alpha^2\pi^2)/Pe + Pe/4$.

Equation (3.5) is formally analogous to the well-known relationship yielding the effective dispersion coefficient D_{eff} predicted by Taylor–Aris theory (Taylor 1953, 1954; Aris 1956). However, the analogy is purely coincidental. Before analysing the behaviour of the Frobenius eigenvalue associated with a generic profile $u(y)$, we explore this point in some detail.

The Taylor–Aris dispersion coefficient quantifies a convection-enhanced dispersion phenomenon that can be observed in pipes or ducts where the velocity profile satisfies no-slip boundary conditions. The no-slip conditions make the axial velocity non-uniform in the channel cross-section. Suppose a scalar pulse is injected at the inlet. In such conditions, consider the scalar profile averaged over the pipe (or the duct) cross-section in a reference frame that moves downstream with the average bulk velocity of the flow. Taylor–Aris theory predicts that in this frame the solution of the cross-averaged advection–diffusion equation possesses dispersion properties which are asymptotically equivalent to those of a pure diffusion equation with an effective diffusivity coefficient D_{eff} given by $D_{\mathrm{eff}} = D + W^2 V_c^2/(192D)$. In dimensionless terms, this implies that for sufficiently large t (or, equivalently far enough from the inlet), the effective Péclet number $Pe_{\mathrm{eff}} = V_c L/D_{\mathrm{eff}}$ should depend on the Péclet number Pe according to the equation

$$\frac{1}{Pe_{\mathrm{eff}}} = \frac{1}{Pe} + \frac{Pe}{192\alpha^2}, \tag{3.6}$$

which is structurally similar to (3.5), since it consists of the combination of two terms, one proportional to Pe, and the other to the reciprocal of Pe. However, this analogy

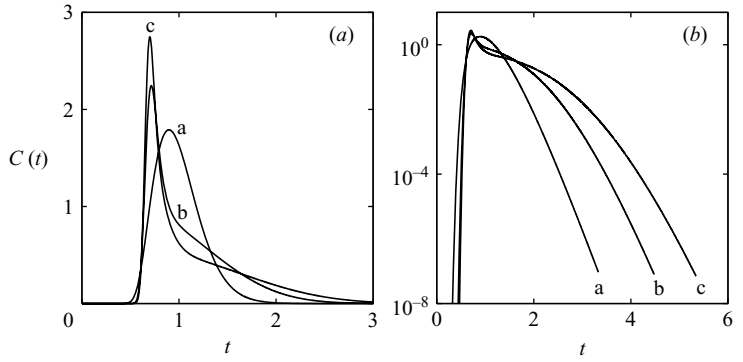

FIGURE 1. Outlet average concentration $C(t)$ *vs* t, the solution of (2.1) for a parabolic velocity profile and an impulsive inlet condition for $\alpha = 5$. (*a*) Normal scale, (*b*) log-normal plot. Line (i) refers to $Pe = 10^2$, line (ii) to $Pe = 5 \times 10^2$, line (iii) to $Pe = 10^3$.

is purely formal, since the plug flow is the only parallel flow for which Taylor–Aris theory provides the trivial result $Pe_{\text{eff}} = Pe$.

The essence of the Taylor–Aris dispersion phenomenon is that flow non-uniformities over the cross-section induce a non-monotonic behaviour of the variance of the concentration pulse with respect to the diffusion coefficient. However, in the case of plug flow, $u(y) = V_c = \text{constant}$, such a phenomenon never occurs as discussed above.

Therefore, the relaxation dynamics (expressed by the behaviour of the Frobenius eigenvalue) and Taylor–Aris dispersion should be considered as two distinct and complementary phenomena in that they refer to different physical situations and to different fluid dynamic problems associated with the interplay between advection and diffusion in channels.

This observation is made clear by the analysis of the 'chromatographic experiments' depicted in figures 1(*a*) and 1(*b*). Figure 1 depicts the outlet average concentration $C(t) = \int_0^1 \phi(1, y, t)\, dy$ solution of Eq. (2.1) for $\phi|_{t=0} = 0$, $\phi|_{x=0} = \delta(t)$, where $\delta(t)$ is an impulsive Dirac distribution for a two-dimensional Poiseuille flow, $u(y) = 6y(1 - y)$ (the prefactor of this parabolic profile stems from the normalization condition $\int_0^1 u(y)\, \mathrm{d}y = 1$).

While Taylor–Aris theory concerns with the broadening of the outlet concentration profile, i.e. the variance of the average $C(t)$ as a function of time t (see figure 1*a*), the analysis of the relaxation properties focuses on the exponential scaling of the tail of the outlet average concentration profile (figure 1*b*), and on how this tail depends on the Péclet number and on the flow profile.

4. Spectral theory of open flows and universality

This Section addresses the spectral properties of the advection–diffusion operator associated with generic open bounded flows. The theoretical analysis developed in this section is not limited to parallel flows but applies to generic laminar flows in channels and ducts. The focus is the behaviour of the dominant Frobenius eigenvalue, the solution of the real eigenvalue problem

$$-\Lambda_F \psi_F = -\nabla \cdot (\boldsymbol{v} \psi_F) + \varepsilon \nabla^2 \psi_F \,, \tag{4.1}$$

subject to the homogeneous boundary conditions:

$$\psi_F|_{\mathscr{S}_i} = 0\,, \qquad \left.\frac{\partial \psi_F}{\partial n}\right|_{\mathscr{S}_o \cup \mathscr{S}_c} = 0\,, \tag{4.2}$$

where $\partial/\partial n = \boldsymbol{n}\cdot\nabla$ indicates the normal derivative and $\boldsymbol{n}$ is the unit normal vector, pointing out of the flow domain Ω. In (4.1), $\mathscr{S}_i$, $\mathscr{S}_c$ and $\mathscr{S}_o$ denote the inlet section, the channel walls, and the outlet section, respectively.

Equation (4.1) is a dimensionless formulation obtained by rescaling all the spatial coordinates by a single characteristic length scale. advection–diffusion in parallel channel flows, i.e. the properties of the eigenvalues of the operator $\mathscr{L}_{\boldsymbol{v},\varepsilon,\alpha}$, is addressed as a particular case at the end of § 4.1.

For the velocity field, we assume the following conditions: (i) $\boldsymbol{v}$ is incompressible, (ii) $\boldsymbol{v} = \boldsymbol{v}(\boldsymbol{x})$ is autonomous, i.e. it does not depend on time, (iii) the outward normal component of the velocity at the outlet section is non-negative.

The Frobenius eigenvalue/eigenfunction has been estimated numerically by solving (1.1) by means of a finite-volume scheme in the presence of the homogeneous boundary conditions (4.2), starting from a generic initial profile, and by applying the iterative power method (Mathews & Fink 2004) to the concentration profiles so obtained. The time advancement was obtained through a second-order explicit algorithm. A total number of cells $N_c = M \times N$ up to $M = 4 \times 10^3$ and $N = 5 \times 10^2$ was used to ensure independence of the results from the discretization.

4.1. *The Frobenius eigenvalue*

By integrating the left- and right-hand sides of (4.1) over the flow domain, one obtains

$$-\Lambda_F \int_\Omega \psi_F \mathrm{d}\boldsymbol{x} = -\int_\Omega \nabla\cdot(\boldsymbol{v}\psi_F)\mathrm{d}_{\boldsymbol{x}} + \varepsilon \int_\Omega \nabla^2\psi_F \,\mathrm{d}\boldsymbol{x}. \tag{4.3}$$

Since ψ_F can always be chosen non-negative, the integral on the left-hand side is positive. For the two integrals entering the right-hand side of (4.3), the application of the divergence theorem and the use of the boundary conditions (4.2) provide the following relations:

$$\int_\Omega \nabla\cdot(\boldsymbol{v}\psi_F)\mathrm{d}\boldsymbol{x} = \int_{\mathscr{S}_o} \psi_F v_n \mathrm{d}S, \qquad \int_\Omega \nabla^2\psi_F \mathrm{d}\boldsymbol{x} = \int_{\mathscr{S}_i} \frac{\partial \psi_F}{\partial n}\,\mathrm{d}S, \tag{4.4}$$

where $v_n = \boldsymbol{v}\cdot\boldsymbol{n}$ is the normal outward component of the velocity. By substituting (4.4) into (4.3), the following relation for Λ_F is obtained:

$$\Lambda_F = \left(\int_\Omega \psi_F \mathrm{d}\boldsymbol{x}\right)^{-1} \left[\int_{\mathscr{S}_o} \psi_F v_n \mathrm{d}S - \varepsilon \int_{\mathscr{S}_i} \frac{\partial \psi_F}{\partial n}\mathrm{d}S\right]\,. \tag{4.5}$$

Another useful relation for Λ_F can be obtained by multiplying (4.1) by ψ_F and integrating over the flow domain Ω. It follows that

$$\int_\Omega \psi_F\, \nabla\cdot(\boldsymbol{v}\psi_F)\,\mathrm{d}\boldsymbol{x} = \frac{1}{2}\int_\Omega \nabla\cdot(\boldsymbol{v}\psi_F^2)\,\mathrm{d}\boldsymbol{x} = \frac{1}{2}\int_{\partial\Omega} \psi_F^2 \boldsymbol{v}\cdot\boldsymbol{n}\,\mathrm{d}S = \frac{1}{2}\int_{\mathscr{S}_o} \psi_F^2 v_n\,\mathrm{d}S \tag{4.6}$$

and

$$\begin{aligned}\int_\Omega \psi_F \nabla^2\psi_F\,\mathrm{d}\boldsymbol{x} &= \int_\Omega \nabla\cdot(\psi_F\,\nabla\psi_F)\,\mathrm{d}\boldsymbol{x} - \int_\Omega |\nabla\psi_F|^2\,\mathrm{d}\boldsymbol{x} \\ &= \int_{\partial\Omega} \psi_F\,\frac{\psi_F}{\partial n}\,\mathrm{d}S - \int_\Omega |\nabla\psi_F|^2\,\mathrm{d}\boldsymbol{x} = -\int_\Omega |\nabla\psi_F|^2\,\mathrm{d}\boldsymbol{x},\end{aligned} \tag{4.7}$$

where the surface integral entering the right-hand side of (4.7) vanishes since either ψ_F (on $\mathscr{S}_i$) or the normal derivative $\partial\psi_F/\partial n$ (on $\mathscr{S}_o \cup \mathscr{S}_c$) is zero at the boundary $\partial\Omega$. Collecting these expressions, one obtains for Λ_F the relation

$$\Lambda_F = \left(\|\psi_F\|_{L^2}^2\right)^{-1} \left[\frac{1}{2}\int_{\mathscr{S}_o} \psi_F^2 v_n \mathrm{d}S + \varepsilon \|\nabla\psi_F\|_{L^2}^2\right], \tag{4.8}$$

where $\|\psi_F\|_{L^2}$ indicates the L^2-norm of the eigenfunction ψ_F, and $\|\nabla\psi_F\|_{L^2}$ the L^2-norm of its gradient,

$$\|\psi_F\|_{L^2}^2 = \int_\Omega \psi_F^2(\boldsymbol{x})\,\mathrm{d}\boldsymbol{x}, \qquad \|\nabla\psi_F\|_{L^2}^2 = \int_\Omega |\nabla\psi_F(\boldsymbol{x})|^2\,\mathrm{d}\boldsymbol{x}. \tag{4.9}$$

Since $v_n|_{\mathscr{S}_o} \geqslant 0$, (4.8) shows that Λ_F is always positive, and therefore the dominant eigenvalue $-\Lambda_F$ is always negative, as required by the dissipative nature of the advection–diffusion operator in bounded open flows.

In the case of two-dimensional channel flows, for which the advection–diffusion operator is given by (2.1), equations (4.5) and (4.8) simplify to

$$\Lambda_F = \left(\int_0^1 \mathrm{d}x \int_0^1 \psi_F \mathrm{d}y\right)^{-1} \left[\int_0^1 u(y)\,\psi|_{x=1}\,\mathrm{d}y - \varepsilon\int_0^1 \left.\frac{\partial\psi_F}{\partial x}\right|_{x=0} \mathrm{d}y\right] \tag{4.10}$$

and

$$\Lambda_F = \left(\|\psi_F\|_{L^2}^2\right)^{-1} \left[\frac{1}{2}\int_0^1 u(y)_F^2\big|_{x=1}\mathrm{d}y + \varepsilon\|\nabla_\alpha\psi_F\|_{L^2}^2\right], \tag{4.11}$$

where $\|\nabla_\alpha\psi_F\|_{L^2}^2 = \int_0^1 \mathrm{d}x \int_0^1 [(\partial\psi_F/\partial x)^2 + \alpha^2(\partial\psi_F/\partial y)^2]\,\mathrm{d}y$.

4.2. *Localization and universality*

Let us apply the approach outlined above to a simple physically realizable flow, namely plane Poiseuille flow defined in a channel. In dimensionless form, the velocity profile is then given by $u(y) = 6y(1-y)$. Figure 2(a, b) shows the dominant Frobenius eigenfunction ψ_F (normalized to possess unit L^2-norm) for two values of the Péclet number. As can be observed, the Frobenius eigenfunction is localized at a boundary layer near the channel walls where the velocity vanishes. As the Péclet number increases (from $Pe = 10^2$ to $Pe = 10^3$, see figure 2) the Frobenius eigenfunction becomes more localized towards the outlet section and closer to the channel walls (note that figure 2b has a different scale than figure 2a). This phenomenon is clearly observable in the data depicted in figure 3(a, b), showing the localization properties of the Frobenius eigenfunction close to the outlet section for a broad range of Pe values.

The spatial structure of the eigenfunctions depicted in figure 3(a, b) suggests a global invariant rescaling of the Frobenius eigenfunctions at high Pe values into a single master function Ψ_F^*. Let $z = 1 - x$, and $\psi_{F,\varepsilon}(z, y)$ be the normalized (to unit L^2 norm) Frobenius eigenfunction for the value ε of the reciprocal Péclet number. The following invariant rescaling is proposed:

$$\psi_{F,\varepsilon}(z, y) = A^{-1}(\varepsilon)\Psi_F^*(z/\beta_1(\varepsilon), y/\beta_2(\varepsilon)) \tag{4.12}$$

where $\beta_1(\varepsilon)$ and $\beta_2(\varepsilon)$ are functions of ε, and $A^{-1}(\varepsilon)$ is the normalization constant. This means that the Frobenius eigenfunctions collapse onto the master function

$$\Psi_F^*(z, y) = A(\varepsilon)\psi_{F,\varepsilon}(\beta_1(\varepsilon)z, \beta_2(\varepsilon)y), \tag{4.13}$$

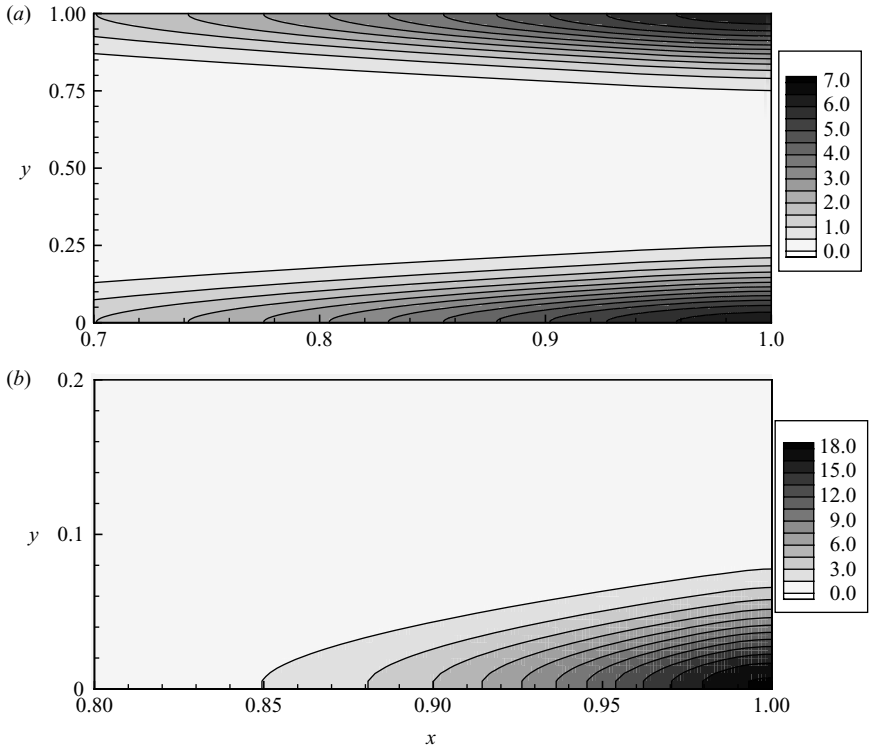

FIGURE 2. Contour plots of the Frobenius eigenfunction for a planar parabolic flow, $\alpha = 1$. (*a*) $Pe = 10^2$. (*b*) $Pe = 10^3$, snapshot close to the outlet section.

at high Pe values. The result of this rescaling is depicted in figure 3(*c*, *d*) by using $\beta_2(\varepsilon) = \beta_1(\varepsilon) \sim \varepsilon^{1/2}$, and the rescaled coordinates $z^* = \beta_1(\varepsilon)(1 - x)$, $y^* = \beta_2(\varepsilon)y$. Henceforth, without loss of generality, $\beta_1(\varepsilon) = \beta_2(\varepsilon) = \beta(\varepsilon) = \varepsilon^{1/2}$ can be assumed. This assumption is required only to simplify the notation and obtaining the scaling of Λ_F with Pe in the simplest possible way. A discussion on the behaviour of $\beta_1(\varepsilon)$ and $\beta_2(\varepsilon)$ as a function of the aspect ratio α is developed in § 5.

The localization of the Frobenius eigenfunctions near the regions of vanishing velocity suggests the existence of universal behaviour for the Frobenius eigenvalue as a function of the Péclet number, namely the fact that the structure of the Frobenius eigenfunction and the scaling of the Frobenius eigenvalue depend exclusively on the local properties of the velocity field close to the channel walls, i.e. close to the stagnation points of the velocity field. Specifically, this invariant rescaling can be used for predicting the behaviour of Λ_F as a function of Pe for different classes of parallel flows.

In order to explore this point in some detail, consider the family of simple parallel flows $u(y) = U_0 y^\nu$, where $U_0 = 1 + \nu$ is a normalization factor, and ν is a nonlinearity exponent controlling the behaviour of the velocity close to lower wall $y = 0$. The plug flow corresponds to $\nu = 0$, and linear shear flow to $\nu = 1$.

By substituting (4.12) into (4.5), and enforcing the localization behaviour of the eigenfunctions near the outlet section, it follows that the surface integral over $\mathscr{S}_i$ appearing in (4.5) can be neglected. Regarding the remaining two integrals entering

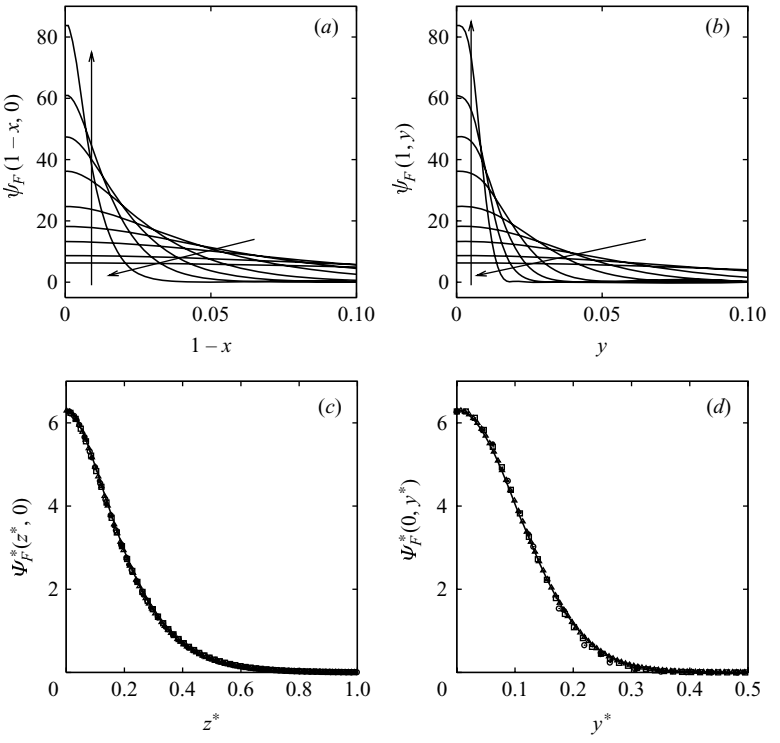

FIGURE 3. Normalized Frobenius eigenfunction for the parabolic profile $u(y)=6y(1-y)$, $\alpha=1$. (*a*) $\psi_F(1-x,0)$ *vs* $1-x$. (*b*) $\psi_F(1,y)$ *vs* y. The arrows indicate increasing values of the Péclet number $3Pe/2=10^2, 2\times10^2, 5\times10^2, 10^3, 2\times10^3, 5\times10^3, 10^4, 2\times10^4, 5\times10^4$. (*c*) Ψ_F^* *vs* $z^*=\beta_1(\varepsilon)(1-x)$ for the curves reported in (*a*). (*d*) Ψ_F^* *vs* $y^*=\beta_1(\varepsilon)y$ for the curves reported in (*b*). Symbols (□, ●, ○, △) refer to the different curves shown in (*a*, *b*) for $3Pe/2=2\times10^2, 10^3, 10^4, 2\times10^4$, respectively.

(4.5), it follows that

$$\int_{\mathscr{S}_o} v_n\psi_{F,\varepsilon}\,\mathrm{d}S = U_0\,A^{-1}(\varepsilon)\int_0^1 y^{\nu}\Psi_F^*(0,y/\beta(\varepsilon))\,\mathrm{d}y. \tag{4.14}$$

By performing the change of variable $\eta=y/\beta(\varepsilon)$, and by observing that as $\varepsilon\to0$ the new upper integration limit $1/\beta(\varepsilon)$ can be approximated by ∞ (due to localization and to the fact that $\lim_{\varepsilon\to0}\beta(\varepsilon)=0$), one finally obtains

$$\int_{\mathscr{S}_o} v_n\psi_{F,\varepsilon}\,\mathrm{d}S = U_0\,A^{-1}(\varepsilon)\beta^{\nu+1}(\varepsilon)\,C_1, \qquad C_1=\int_0^\infty \eta^{\nu}\Psi_F^*(0,\eta)\,\mathrm{d}\eta. \tag{4.15}$$

By enforcing (4.12) in the denominator of (4.5), one obtains

$$\int_\Omega \psi_F\,\mathrm{d}\boldsymbol{x} = A^{-1}(\varepsilon)\,\beta^2(\varepsilon)\,C_0\,, \qquad C_0=\int_0^\infty\int_0^\infty \Psi_F^*(\xi,\eta)\,\mathrm{d}\xi\,\mathrm{d}\eta. \tag{4.16}$$

Collecting (4.15) and (4.16) and substituing them into (4.5), if follows that

$$\Lambda_F = D_1\beta^{\nu-1}(\varepsilon), \tag{4.17}$$

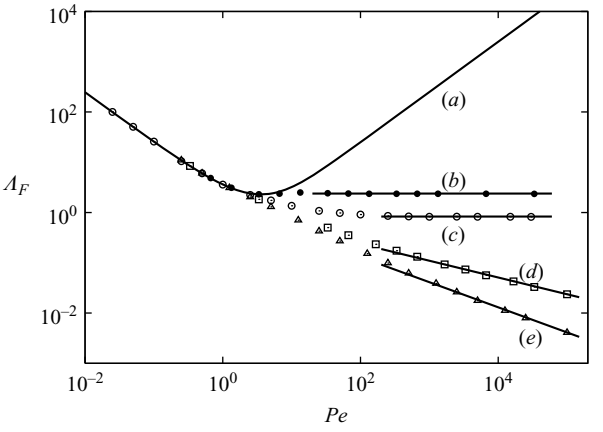

FIGURE 4. Frobenius eigenvalue Λ_F *vs* Pe, $\alpha = 1$. Line (*a*) refers to the plug flow and is the graph of (3.5), line (*b*) and ● to the parabolic flow, line (*c*) and ○ to the planar shear flow $u(y) = 2y$, line (*d*) and □ to the 'quadratic shear flow' $u(y) = 3y^2$, line (*e*) and △ to the 'cubic' shear flow $u(y) = 4y^3$. Lines (*d*) and (*e*) correspond to the scalings $\Lambda_F \sim Pe^{-1/3}$, $\Lambda_F \sim Pe^{-1/2}$, respectively.

where $D_1 = U_0 C_1 / C_0$. The same approach can be applied to the integrals entering (4.8). Specifically,

$$\|\psi_{F,\varepsilon}\|_{L^2}^2 = A^{-2}(\varepsilon) C_4 / \beta^2(\varepsilon), \qquad \text{where } C_4 = \|\Psi_F^*\|_{L^2}^2, \tag{4.18}$$

$$\int_{\mathscr{S}_o} \psi_{F,\varepsilon}^2 v_n \mathrm{d}s = U_0 A^{-2}(\varepsilon) C_2 \beta^{\nu+1}(\varepsilon), \qquad \text{where } C_2 = \int_0^\infty y^2 [\Psi_F^*(0,\eta)]^2 \,\mathrm{d}\eta, \tag{4.19}$$

and

$$\|\nabla \psi_{F,\varepsilon}\|_{L^2}^2 = A^{-2}(\varepsilon) C_3, \qquad \text{where } C_3 = |\nabla \Psi_F^*|_{L^2}^2. \tag{4.20}$$

By substituting these expressions (4.18)–(4.20) in (4.8), it follows that

$$\Lambda_F = D_2 \beta^{\nu-1}(\varepsilon) + D_3 \frac{\varepsilon}{\beta^2(\varepsilon)}, \tag{4.21}$$

where $D_2 = U_0 C_2 / 2C_4$ and $D_3 = C_3 / C_4$. By comparing (4.17) and (4.21), it follows that

$$D_1 \beta^{\nu-1}(\varepsilon) = D_2 \beta^{\nu-1}(\varepsilon) + D_3 \frac{\varepsilon}{\beta^2(\varepsilon)} \quad \Rightarrow \quad \beta(\varepsilon) = K \varepsilon^{1/(1+\nu)} \tag{4.22}$$

where $K = [D_3/(D_1 - D_2)]^{1/(\nu+1)}$ is a constant. By substituting (4.22) into (4.17) the following scaling of the Frobenius eigenvalue with respect to the Péclet number can be derived:

$$\Lambda_F \simeq \beta^{\nu-1}(\varepsilon) \sim \varepsilon^{(\nu-1)/(1+\nu)} = Pe^{\gamma}, \qquad Pe \gg 1, \tag{4.23}$$

where the exponent γ is given by

$$\gamma = \frac{1-\nu}{1+\nu}. \tag{4.24}$$

The results for the plug flow ($\nu = 0$, $\gamma = 1$) are consistent with the analytic expression (3.5) for Λ_F. Figure 4 shows the comparison, for different parallel flows, of the theoretical scaling (4.23) (bold lines *b–e*) and the results obtained through numerical simulations (symbols).

At small Pe ($Pe < 1$), the scaling of Λ_F is independent of the flow profile, and is controlled exclusively by diffusion, leading to the scaling $\Lambda_F \sim Pe^{-1}$. At high values, $Pe \geqslant 10^2$, numerical simulations are consistent with the theory. The planar shear flow $u(y) = 2y$ and the planar Poiseuille flow $u(y) = 6y(1-y)$ yield $\Lambda_F \sim$ constant, i.e. $\gamma = 0$ as predicted by (4.23). Figure 4 shows also the behaviour of Λ_F for two other model flows, namely the quadratic ($u(y) = 3y^2$, i.e. $\nu = 2$), and the cubic shear flow ($u(y) = 4y^3$, i.e. $\nu = 3$). The theory predicts $\gamma = -1/3$ for $\nu = 2$, and $\gamma = -1/2$ for $\nu = 3$ which is in perfect agreement with the results of numerical simulations.

Equations (4.23)–(4.24) are the main results of this article. Equation (4.24) shows that the scaling exponent γ, which controls the behaviour of the Frobenius eigenvalue at high Pe values, depends exclusively on the local behaviour of the velocity field near the stagnation points, and specifically on the order of nonlinearity ν of the flow. Equation (4.24) implies a universal behaviour of the Frobenius eigenvalue with respect to the structure of the flow field. In fact the exponent γ does not depend on the fine details of the flow field but exclusively on the nonlinearity exponent ν near the stagnation points. This result is conceptually analogous to what observed in closed flow systems (Giona *et al.* 2004*b*), where the scaling exponent of the dominant non-vanishing eigenvalue of the advection–diffusion operator depends on the local behaviour of the velocity field near its critical points.

4.3. *Simple electro-osmotic flows*

In the previous section we have considered the spectral properties of two-dimensional Poiseuille flow and of the family of generalized shear flows $u(y) = U_0 y^{\nu}$. Only the case $\nu = 1$ of this family corresponds to a physically realizable flow. Even though these model flows for $\nu > 1$ are not physically realizable, their consideration was aimed at validating the theoretical prediction based on the eigenfunction localization expressed by (4.23). In fact, quadratic nonlinearities near stagnation points of the velocity profile can occur in some electro-osmotic flows.

Consider the case of an electro-osmotic flow in a two-dimensional straight micro-channel. By making use of the Poisson–Boltzmann equation with the Debye–Hückel approximation (Karniandakis, Beskok & Aluru 2005; Kandlikar *et al.* 2006), the electrostatic potential $\phi_e(y)$ is the solution of the linear equation $\mathrm{d}^2\phi_e(y)/\mathrm{d}y^2 = \kappa^2\phi_e(y)$, where κ is the reciprocal of the dimensionless Debye length, with the boundary conditions $\phi_e(y=0) = \phi_e(y=1) = \zeta$, ζ being the zeta-potential of the material forming the channel walls.

In the presence of a pressure drop opposing the action of the electro-osmotic forcing term, the dimensionless velocity profile $u(y)$, the solution of the Navier–Stokes equation with no-slip boundary condition at the walls is (Karniadakis *et al.* 2005)

$$u(y) = C[1 - A(\kappa)\mathrm{e}^{\kappa x} + B(\kappa)\mathrm{e}^{-\kappa x} + (\Delta\pi_s)y(1-y)] = C[u_{eo}(y) + (\Delta\pi_s)y(1-y)] \quad (4.25)$$

where κ is the reciprocal of the dimensionless length of the electric double layer, $\Delta\pi_s$ is the dimensionless pressure drop, $A(\kappa) = (1-\mathrm{e}^{-\kappa})/(\mathrm{e}^{\kappa} - \mathrm{e}^{-\kappa})$, $B(\kappa) = (\mathrm{e}^{\kappa} - 1)/(\mathrm{e}^{\kappa} - \mathrm{e}^{-\kappa})$, and C is a normalization constant so that $\int_0^1 u(y)\,\mathrm{d}y = 1$.

By adjusting the pressure drop for fixed κ it is possible to obtain a stagnation point in the middle of the channel section. This situation is depicted in figure 5(*a*) for $\kappa = 50$ and $\Delta\pi_s = -4.0$.

The flow field $u(y)$ depicted in figure 5(*a*) possesses three stagnation points on the cross-section of the channel. Two stagnation points, corresponding to the channel walls $y = 0, 1$, are induced by the no-slip boundary conditions, and are characterized

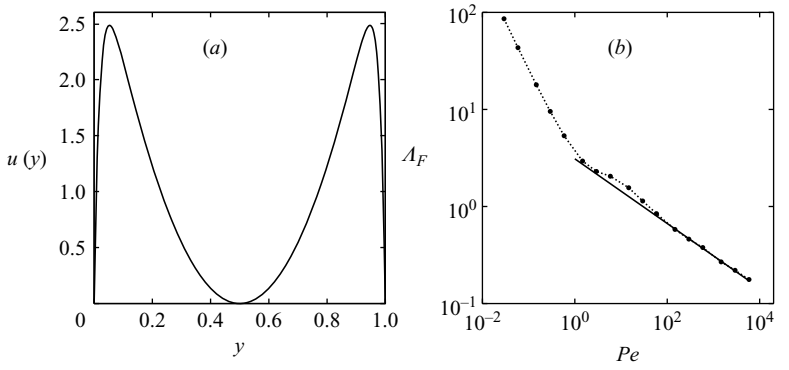

FIGURE 5. (*a*) Electro-osmotic flow profile (4.25) with $\kappa = 50$, $\Delta\pi_s = -4.0$. (*b*) Frobenius exponent Λ_F *vs* Pe for the electro-osmotic flow depicted in (*a*) for $\alpha = 1$. The solid line corresponds to the theoretical scaling $\Lambda \sim Pe^{-1/3}$.

by a linear behaviour of the velocity, i.e. $\nu = 1$. The remaining stagnation point is located in the middle of the channel $y_c = 1/2$ and is characterized by a quadratic nonlinearity $\nu = 2$, i.e. $u(y) = \text{const}(y - y_c)^2$ in the neighbourhood of y_c.

From the universal theory developed in the previous Section, it is expected that: (i) the behaviour close to the stagnation point possessing the higher nonlinearity exponent ν will control the asymptotic scaling of the Frobenius eigenvalue, since it is associated with the slowest decay rate, and (ii) the Frobenius eigenfunction will be localized in the neighbourhood of this stagnation point. In the present case, since $\nu = 2$, the scaling $\Lambda_F \sim Pe^{-1/3}$ is theoretically expected, and the dominant Frobenius eigenfunction should be localized in the neighbourhood of the channel mid-point (and not close to the walls).

The results of the numerical simulations for the scaling of the Frobenius eigenvalue are depicted in figure 5(*b*), and shown agreement with the theoretical scaling (4.23)–(4.24).

The spatial structure of the Frobenius eigenfunctions for this model flow is depicted in figure 6 and in figure 7 (contour plot). As predicted by the theory, the Frobenius eigenfunctions become progressively localized close to $y_c = 1/2$, which is the stagnation point associated with the slowest decay rate. This example provides a simple and physically relevant confirmation of the theory, and motivates the use of the generalized shear flows discussed in the previous Section.

5. Further observations

The result expressed by (4.23) is valid for generic two- and three-dimensional laminar flows. For instance, Poiseuille flow in a cylindrical pipe ($\nu = 1$) yields $\Lambda_F \sim$ constant for high Pe, and this is confirmed by numerical simulations (not shown for brevity).

Let us briefly consider the effect of the aspect ratio α on the dominant eigenvalue of the spectrum of the advection–diffusion operator. Figure 8 shows the behaviour of the Frobenius eigenvalue for two-dimensional Poiseuille flow for different values of α. As expected, the asymptotic scaling is independent of the aspect ratio, while the saturation value of Λ_F increases monotonically with α.

As α increases, the envelope of the graph of Λ_F as a function of Pe approaches the behaviour of the Frobenius eigenvalue of the plug flow (compare line (*d*) with

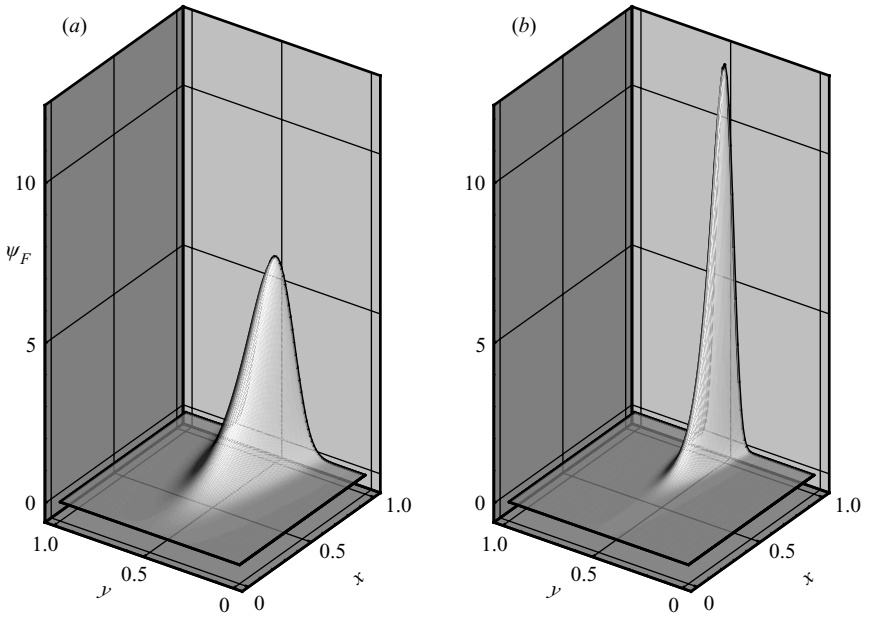

FIGURE 6. Spatial structure of the Frobenius eigenfunctions associated with the electro-osmotic flow (4.25) with $\kappa = 50$, $\Delta\pi_s = -4.0$, $\alpha = 1$. (*a*) $Pe = 0.3 \times 10^3$, (*b*) $Pe = 0.3 \times 10^4$.

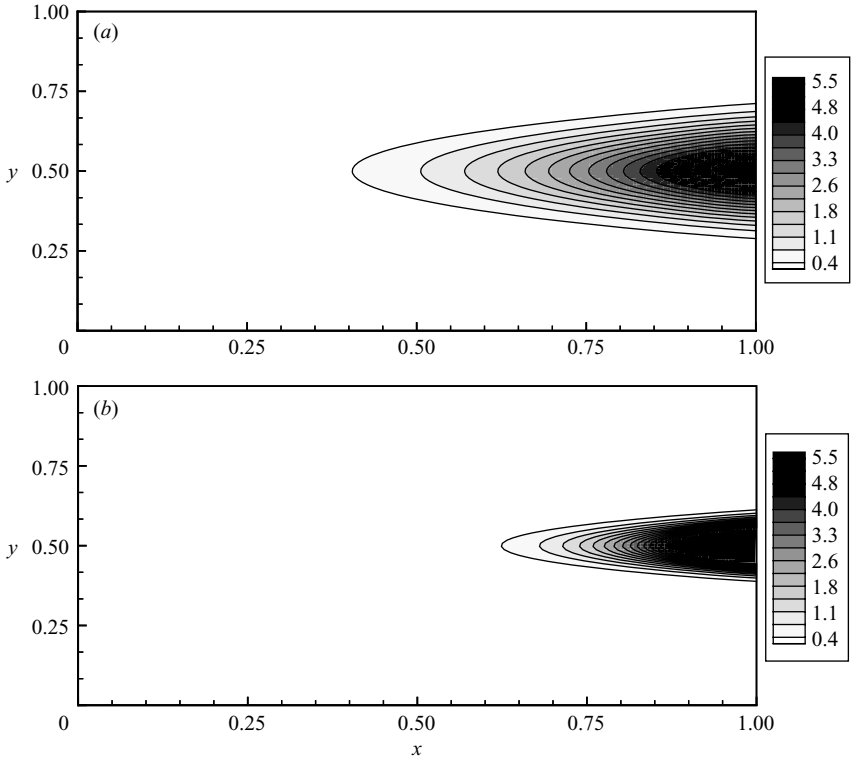

FIGURE 7. Contour plot of the Frobenius eigenfunctions depicted in figure 6. (*a*) $Pe = 0.3 \times 10^3$, (*b*) $Pe = 0.3 \times 10^4$.

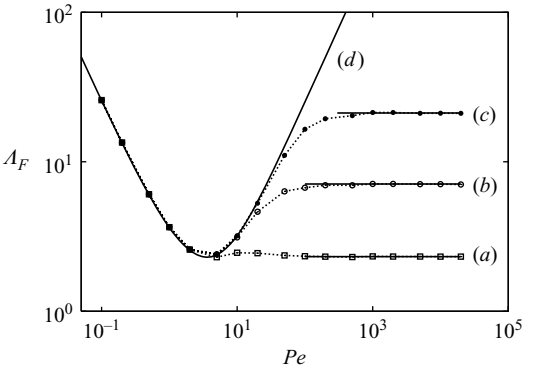

FIGURE 8. Frobenius eigenvalue Λ_F *vs* Pe for the two-dimensional Poiseuille flow for different values of the aspect ratio α. Line (*a*) and □ refers to $\alpha^2 = 1$, line (*b*) and ○ to $\alpha^2 = 10$, line (*c*) and ● to $\alpha^2 = 10^2$. Line (*d*) depicts the Frobenius eigenvalue for the plug flow (3.5).

lines (*b*) and (*c*) in figure 8). This phenomenon can be expected, since for α tending to infinity, the concentration profile, the solution of the dimensionless advection–diffusion equation (2.1), becomes uniform over each cross-section, and the influence of the non-uniformities in the velocity profile becomes immaterial. This observation is confirmed by the spatial structure of the eigenfunctions, a contour plot of which are depicted in figure 9(*a*) for $\alpha = 10^2$. For $Pe \leqslant 50$, i.e. for values of the Péclet number for which Λ_F is close to the plug-flow value (see figure 8, line *c*), the eigenfunctions admit a global support coinciding with the whole cross-section of the tube, and approximate the Frobenius eigenfunction of the plug flow $\psi_F(x, y) = \mathrm{e}^{Pex/2} \sin(\omega_1 x)$. For higher values of Pe, eigenfunction localization close to the outlet walls becomes significant (see figure 9*b*), and this leads to the saturation behaviour of Λ_F with Pe.

Let us analyse quantitatively the influence of the aspect ratio on the behaviour of Λ_F. In performing this analysis, the different dependence of $\beta_1 = \beta_1(\varepsilon, \alpha)$ and $\beta_2 = \beta_2(\varepsilon, \alpha)$ entering (4.12) on α should be explicitly accounted for. The results of the numerical simulations suggest that β_1 and β_2 can be expressed as

$$\beta_1(\varepsilon, \alpha) = \beta_{1,0}\, b(\varepsilon), \qquad \beta_2(\varepsilon, \alpha) = \beta_{2,0}\, \alpha\, b(\varepsilon) \tag{5.1}$$

where $b(\varepsilon)$ is a function exclusively of ε. By enforcing (5.1) in the integral equations for Λ_F one obtains, in place of (4.17) the expression

$$\Lambda_F = D_1 \frac{\beta_2^{\nu}}{\beta_1} = \widetilde{D_1}\, \alpha^{\nu}\, b^{\nu-1}(\varepsilon) \tag{5.2}$$

where $\widetilde{D}_1 = D_1(b_{2,0}^{\nu}/b_{1,0})$, which indicates that for $\alpha \gg 1$, $\Lambda_F \sim \alpha^{\nu}$. This result is consistent with the closed form expression for the plug flow ($\nu = 0$), (3.5), where Λ_F is independent of α and for the Pouiseuille flow, for which Λ_F for large Pe scales linearly with α (the analysis of the saturation values of Λ_F depicted in figure 8 confirms this observation).

It is important to analyse the robustness of (4.23) both with respect to the nature of the boundary conditions and the presence of velocity perturbations. As it concerns the boundary conditions, we made use of the inlet condition $\psi|_{\mathscr{S}_i} = 0$, which corresponds to enforcing continuity of the concentration. A different approach consists of enforcing flux continuity. This leads to the mixed boundary condition at the inlet, $u(y)\psi - \varepsilon \partial\psi/\partial n|_{\mathscr{S}_i} = 0$. At large Pe values (small ε), the two types of boundary conditions

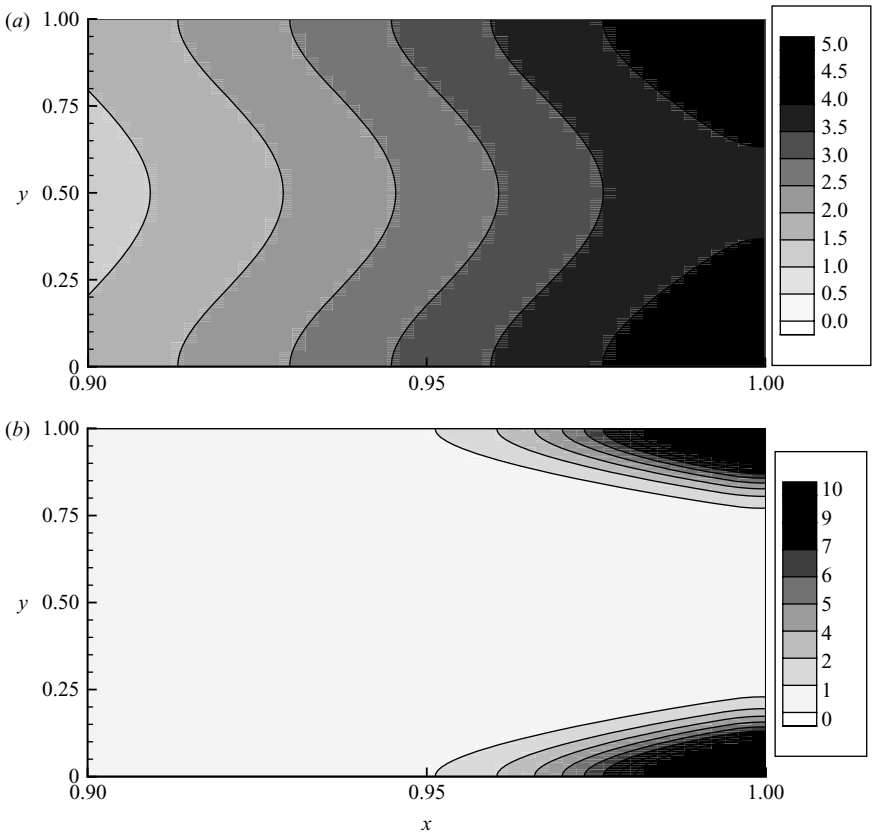

FIGURE 9. Contour plots of the Frobenius eigenfunction for a planar parabolic flow, $\alpha = 10^2$. (*a*) $Pe = 50$. (*b*) $Pe = 10^3$, snapshot close to the outlet section.

are essentially equivalent. This implies that the same scaling expression holds for the Frobenius exponent. In other words, the choice of different inlet boundary conditions modifies the behaviour of Λ_F only at small values of Pe, i.e. when the Frobenius eigenfunction is distributed over large portions of the flow domain. At high values of Pe, the Frobenius eigenfunction becomes localized near the outlet section and consequently the choice of the inlet boundary condition, enforcing either the continuity of the concentration or of the flux, becomes immaterial.

The universal scaling (4.23) is also robust with respect to flow perturbations which alter the parallel nature of the flow. To show this, consider a two-dimensional perturbation of planar Poiseuille flow, generated by the stream function $s(x, y) = (3y^2 - 2y^3)[1 + y^2(1 - y)^2(\cos(2\pi x) + a\cos(6\pi x))]$ for $a = -1/2$ ($u = \partial s/\partial y$, $v = -\partial s/\partial x$). Figure 10(*a*) depicts the streamlines of this flow, while figure 10(*b*) compares its Frobenius eigenvalue with that of planar Poiseuille flow. Even though the advection–diffusion operator in open bounded flows is intrinsically non-normal (Schmid 2007; Chomaz 2005), the universal scaling (4.23) is robust with respect to weak perturbations that destroy the parallel flow structure.

As a final comment, let us discuss a physically relevant application of (4.23) in the context of micro- and nanoflows. One of the open issues in decreasing the length scales below the range of few microns is the occurrence of slip flows at the solid walls. The scaling relation (4.23) provides a simple and experimentally feasible way

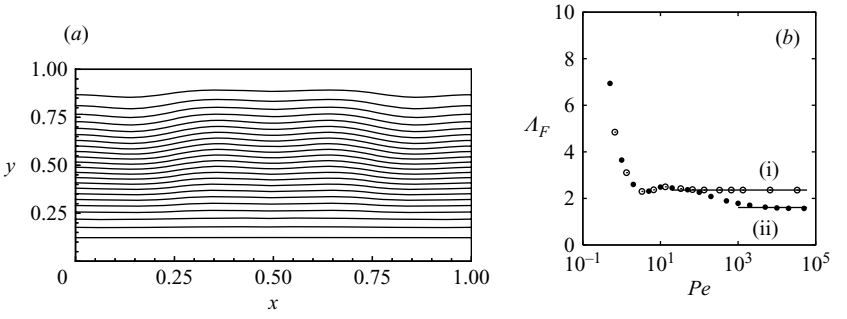

FIGURE 10. (*a*) Streamlines of the perturbed Poiseuille flow generated by the streamfunction $s(x, y)$ with $a = -0.5$. (*b*) Frobenius exponent Λ_F *vs Pe*. Line (i) and ○ planar Poiseuille flow, line (ii) and ● perturbed flow depicted in (*a*).

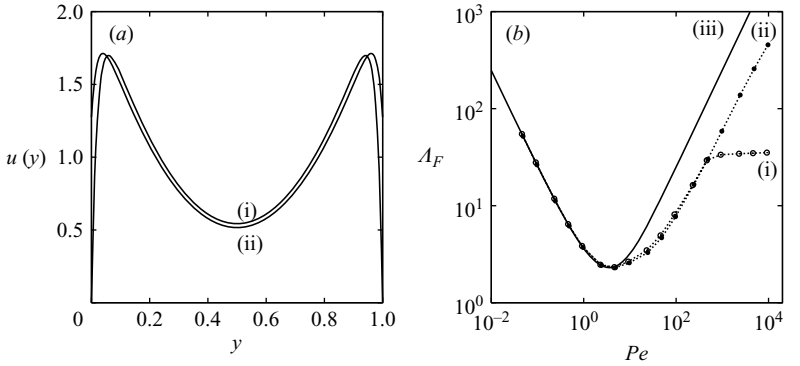

FIGURE 11. (*a*) Electroosmotic flow profile. Line (i) refers to (4.25) with $\kappa = 50$, $\Delta\pi_s = -3$. Line (ii) is a slip-perturbation of the flow profile of line (i), obtained by modifying the electro-osmotic term $\widetilde{u}_{os}(y) = u_{os}((y+\eta)/(1+2\eta))$, with $\eta = 0.02$. (*b*) Frobenius exponent Λ_F *vs Pe* for the electro-osmotic flow (line (i) and ○) and for its slip-perturbation (line (ii) and ●). Line (iii) is the analytical result for the plug flow.

to assess the validity of no-slip boundary conditions or to infer the occurrence of slip velocities. Equation (4.23) or figure 4 indicate that whenever no-slip occurs at the solid walls, the relaxation exponent either saturates or decreases at large *Pe*. Conversely, the occurrence of slip boundary conditions can be inferred whenever the Frobenius eigenvalue increases linearly with *Pe*. This phenomenon is illustrated in figure 11 for the case where an electro-osmotic force is combined with a pressure counter-gradient, (4.25).

Figure 11(*a*) line (i) shows a typical electrokinetic flow profile for $\kappa = 50$ and $\Delta\pi_s = -3$, while curve (ii) depicts a weak perturbation of the flow profile (4.25), namely $\widetilde{u}(y) = C\widetilde{u}_{eo}(y) + (\Delta\pi_s)y(1-y)$, where $\widetilde{u}_{eo}(y) = u_{eo}((y+\eta)/(1+2\eta))$ and $\eta = 0.02$. The perturbed flow $\widetilde{u}(y)$ is close to $u(y)$ but it is characterized by a slip velocity at the channel walls. The behaviour of Λ_F vs *Pe* for these flows is depicted figure 11(*b*). These data confirm the universal scaling expressed by (4.23): while the electro-osmotic flow in the presence of non-slip boundary conditions is characterized by a saturating behaviour of Λ_F with *Pe*, its slip perturbation $\widetilde{u}(y)$ shows a diverging behaviour of Λ_F for high *Pe* values, as observed e.g. in the plug flow. This result indicates that simple experiments on advecting–diffusing scalars (e.g. using a capillary

electrochromatographic column) can in principle be used to discriminate between slip and non-slip conditions in microchannels.

6. Concluding remarks

This article focuses on the time scale characterizing the convergence towards the steady-state profile of a diffusing scalar continuously fed into a finite length channel in the presence of a (possibly non-uniform) velocity profile. The spectral (functional) approach to this problem predicts that the slowest relaxation exponent is given by the Frobenius eigenvalue, $-\Lambda_F$, associated with the advection–diffusion operator with appropriate boundary conditions.

In the case of a flat velocity profile (plug flow), a non-monotonic behaviour of Λ_F as a function of Pe has been derived in closed form. The functional structure of this dependence is formally identical to the relationship, referred to as Taylor–Aris dispersion, yielding the effective axial dispersion coefficient in the presence of a non-uniform flow profile (e.g. Poiseuille flow). However, the Frobenius eigenvalue and the Taylor–Aris dispersion coefficient are distinct quantities, which refer to different physical phenomena.

In the case of non-uniform flow profiles that satisfy no-slip conditions and are locally linear at the channel walls, the behaviour of Λ_F vs. Pe saturates towards a constant value at large Pe. This result can be derived analytically by exploiting the localization property associated with the Frobenius eigenfunction, which, as $Pe \to \infty$, is non-zero only in smaller and smaller areas located at the channel exit and near the static walls (which are stagnation points for the velocity profile).

The localization feature is then analysed in the case where the local behaviour of the velocity profile near the stagnation point is nonlinear. Examples are provided for quadratic and cubic nonlinearities. These examples show that a universal localization behaviour holds for the Frobenius eigenfunction, and that the invariant rescaling ultimately depends on the nonlinearity exponent associated with the velocity profile near the stagnation points. On the basis of the universal localization feature, a closed form expression yielding the high-Pe asymptotic behaviour of Λ_F is derived analytically in terms of the nonlinearity exponent of the velocity profile. Numerical simulations confirm quantitatively the theoretical prediction. A velocity profile possessing a stagnation point characterized by a quadratic nonlinearity, obtained by a pressure drop that opposes an electro-osmotic body force, is considered as an example of physically realizable flow with nonlinear behaviour near a stagnation point far from the channel walls.

The consideration of different values of the channel aspect ratio α for the case of Poiseuille flow shows that this parameter can have a significant impact on the value of Λ_F for high Pe, but not on its asymptotic scaling. Specifically, the curve Λ_F vs. Pe associated with the Poiseuille profile collapses onto the analytical solution associated with the plug flow case within an interval of Pe values of say $Pe = (0, Pe^*(\alpha)]$, where $Pe^*(\alpha) \to \infty$ as $\alpha \to \infty$. This implies that for higher and higher aspect-ratio channels the influence of stagnation points appear only at larger and larger Pe.

Beyond predicting the controlling time scale to reach steady-state conditions in microflow devices, we also suggest a simple if indirect experiment to exploit the knowledge of the asymptotic behaviour of Λ_F vs. Pe to establish the occurrence of slip boundary conditions (physically, deviations from the no-slip condition are mainly expected in gaseous flows, whenever the mean free path becomes comparable with the characteristic dimension of the channel cross-section).

The analysis presented in this article can be considered an extension of the results derived in Giona *et al.* (2004*b*) in the context of closed bounded parallel flows. The main difference in the universal behaviour is that in closed flows the nonlinearity exponent controlling the rate of convergence towards the steady state is associated with the local behaviour of the velocity profile near *critical points* (i.e. relative extremals) whereas in open systems the nonlinearity exponent is that associated with the local behaviour of the velocity profile near stagnation points.

The approach developed in this paper, based on integral and norm conditions expressing Λ_F as a function of the corresponding Frobenius eigenfunction, can be regarded as a boundary-layer-type analysis, resting upon eigenfunction localization. In principle, other analytical methods could be used to investigate the same phenomenon, such as the WKB approximation. However, the WKB approach is neither more rigorous nor more accurate than the integral approach presented here. In fact, it is known that for non-Hermitian operators, such as the advection–diffusion operator, or the non-Hermitian Schrödinger operator introduced in PT-symmetric theories of quantum mechanics (Bender 2007; Dorey, Millican-Slater & Tateo 2005), the WKB approximation can be technically onerous, and in some cases can lead to erroneous conclusions (Dorey, *et al.* 2005). Moreover, the WKB approximation suffers from some specific problems when applied to the analysis of spectral problems associated with fluid mixing systems. While in quantum mechanics, WKB eigenvalues can be obtained by enforcing the Bohr–Sommerfeld quantization conditions, a similar approach cannot be straightforwardly applied in the analysis of the advection–diffusion equations in bounded domains. This makes the application of WKB in this context a challeging and open isssue.

REFERENCES

Aris, R. 1956 On the dispersion of a solute in a fluid flowing through a tube. *Proc. R. Soc. Lond.* A **235**, 67–77.

Backus, G. 1958 A class of self-sustaining dissipative spherical dynamos. *Annals Phys.* **4**, 372–447.

Beigie, D., Leonard, A. & Wiggins, S. 1991 A global study of enhanced stretching and diffusion in chaotic tangles. *Phys. Fluids* A **3**, 1039–1050.

Bender, C. M. 2007 Making sense of non-Hermitians Hamiltonians. *Rep. Prog. Phys.* **70**, 947–1018.

Chertkov, M. & Lebedev, V. 2003 Boundary effects on chaotic advection–diffusion chemical reactions. *Phys. Rev. Lett.* **90**, 134501.

Chomaz, J.-M. 2005 Global instabilities in spatially developing flows: Non-normality and nonlinearity. *Annu. Rev. Fluid Mech.* **37**, 357–392.

Danckwerts, P. V. 1953 Continuous flow systems. *Chem. Engng Sci.* **2**, 1–13.

Dorey, P., Millican-Slater, A. & Tateo, R. Beyond the WKB approximation in PT-symmetric quantum mechanics. *J. Phys.* A **38**, 1305–1331.

Fannjiang, A. & Papanicolaou, G. 1994 Convection enhanced diffusion for periodic flows. *SIAM J. Appl. Maths* **54**, 333–408.

Fannjiang, A. & Papanicolaou, G. 1997 Convection-enhanced diffusion for random flows. *J. Statist Phys.* **88**, 1033–1076.

Farina, L. & Rinaldi, S. 2000 *Positive Linear Systems. Theory and applications.* John Wiley and Sons.

Gilbert, A. D. 2006 Advected fields in maps – III. Passive scalar decay in baker's maps. *Dyn. Syst.* **21**, 25–71.

Giona, M., Adrover, A. & Cerbelli, S. 2005 On the use of the pulsed-convection approach for modelling advection–diffusion in chaotic flows - A prototypical example and direct numerical simulations. *Physica* A **348**, 37–73.

Giona, M., Adrover, A., Cerbelli, S. & Vitacolonna, V. 2004*a* Spectral properties and transport machanisms of partially chaotic bounded flows in the presence of diffusion. *Phys. Rev. Lett.* **92**, 114101.

Giona, M., Cerbelli, S. & Vitacolonna, V. 2004*b* Universality and imaginary potentials in advection–diffusion equations in closed flows. *J. Fluid Mech.* **513**, 221–237.

Kandlikar, S. G., Garimella, S., Li, D., Colin, S. & King, M. R. 2006 *Heat Transfer and Fluid Flow in Minichannels and Microchannels*. Elsevier.

Karniandakis, G., Beskok, A. & Aluru, N. 2005 *Microflows and Nanoflows*. Springer.

Majda, A. J. & Kramer, P. R. 1999 Simplified models for turbulent diffusion: Theory, numerical modelling and physical phenomena. *Phys. Rep.* **314**, 237–574.

Mathews, J. H. & Fink, K. K. 2004 *Numerical Methods using Matlab*. Prentice-Hall.

Pierrehumbert, R. T. 1994 Tracer microstructure in large-eddy dominated regime. *Chaos Solitons Fractals* **4**, 1091–1110.

Pikovsky, A. & Popovych, O. 2003 Persistent patterns in deterministic mixing flows. *Europhys. Lett.* **61**, 625–631.

Popovych, O. V., Pikovsky, A. & Eckhardt, B. 2007 Abnormal mixing of passive scalars in chaotic flows. *Phys. Rev.* E **75**, 036308.

Schmid, P. J. 2007 Nonmodal stability theory. *Annu. Rev. Fluid Mech.* **39**, 129–162.

Smith, R. 1988 Entry and exit conditions for flow reactors. *IMA J. Appl. Maths.* **41**, 1–20.

Straube, A. V. & Pikovsky, A. 2007 Mixing-induced global modes in open active flow. *Phys. Rev. Lett.* **99**, 184503.

Taylor, G. 1953 Dispersion of soluble matter in a solvent flowing slowly through a tube. *Proc. R. Soc. Lond.* A **219**, 186–203.

Taylor, G. 1954 The dispersion of matter in turbulent flow through a pipe. *Proc. R. Soc. Lond.* A **223**, 446–468.

Tel, T., de Moura, A., Grebogi, C. & Karolyi, G. 2005 Chemical and biological activity in open flows: A dynamical system approach. *Phys. Rep.* **413**, 91–196.